PHILOSOPHICAL TRANSACTIONS OF THE ROYAL SOCIETY A MATHEMATICAL, PHYSICAL & ENGINEERING SCIENCES

# The de Haas - van Alphen Effect in Aluminium

E. M. Gunnersen

*Phil. Trans. R. Soc. Lond. A* 1957 **249**, 299-320
doi: 10.1098/rsta.1957.0001

# THE de HAAS – van ALPHEN EFFECT IN ALUMINIUM

By E. M. GUNNERSEN

*Royal Society Mond Laboratory, University of Cambridge*

(*Communicated by D. Shoenberg, F.R.S.—Received* 19 *June* 1956)

The de Haas–van Alphen effect in aluminium has been studied by measuring the oscillatory variation with magnetic field of the torque on a single crystal at liquid-helium temperatures in fields up to 15·4 kG. The torques were measured by an electronic feed-back device designed to reduce the twisting motion of the crystal during torque measurement. Particular attention was paid to the variation of the periods of the relatively high-frequency components of the oscillations with the orientation of the field relative to the crystal axes. A consistent interpretation was obtained by supposing that there are three such periodic components for each field direction, though often the relative amplitude of one or two of these is negligibly small. In terms of Onsager's theory, the period is inversely proportional to the maximum area of cross-section of the Fermi surface by planes normal to the field, and the three periodic components have been shown to correspond to three identical cushion-shaped pieces of the Fermi surface with their principal axes mutually perpendicular. The location of these pieces in relation to the Brillouin zone is discussed and the characteristic dimensions of each piece have been calculated. Some results on the variation of the period of the relatively low-frequency component with field orientation in a (100) plane are described, but no detailed interpretation in terms of the shape of appropriate parts of the Fermi surface has been obtained. A few results on the variation of the oscillation amplitude with field orientation and on the temperature-dependence of amplitude are also presented. Alloying the aluminium with up to 0·26 % magnesium increases the period of the low-frequency component by about 2·3 %; this suggests that this component arises from electrons rather than holes. The period of the high-frequency component is not significantly changed by alloying.

## CONTENTS

| | PAGE |
|---|---|
| 1. Introduction | 299 |
| 2. Experimental details | 301 |
| (*a*) The torque meter apparatus | 301 |
| (*b*) The magnetic field | 302 |
| (*c*) The specimens | 302 |
| 3. Period anisotropy of the high-frequency oscillations | 303 |
| (*a*) Experimental procedure and results | 303 |
| (*b*) Interpretation of the anisotropy of the high-frequency periods | 309 |
| (*c*) Representation of the period anisotropy results on a stereographic plot | 310 |
| (*d*) Calculation of the shape and size of the Fermi surface causing the high-frequency oscillations | 312 |
| 4. Miscellaneous experimental results | 315 |
| (*a*) Period anisotropy of the low-frequency oscillations | 315 |
| (*b*) Anisotropy of the oscillation amplitudes | 316 |
| (*c*) The dependence of oscillation amplitudes on temperature | 317 |
| (*d*) The effect of alloying with magnesium | 318 |
| References | 319 |

## 1. Introduction

At low temperatures many metals show an oscillatory variation of magnetic susceptibility with field, $H$ (the de Haas–van Alphen effect); the period of these oscillations is constant if

they are plotted against $1/H$. Landau (1939) worked out the theory of this effect assuming a quadratic dependence of the energy $E$ of the electrons on momentum $p$ (ellipsoidal energy surfaces in $p$-space), and showed that the period $\Delta(1/H)$ is given by

$$\Delta(1/H) = eh/2\pi mcE_0, \tag{1}$$

where $m$ is an appropriate effective electron mass and $E_0$ is the Fermi energy relative to the highest or lowest energy of the band. Comparison of Landau's theory with experiment (Shoenberg 1939, 1952) confirmed the main qualitative predictions of the theory, but suggested that the ellipsoidal assumption was inadequate for some of the metals studied.

Onsager (1952) discussed the theory for an arbitrary dependence of $E$ upon $p$, and showed that the period $\Delta(1/H)$ should be inversely proportional to the maximum (or minimum)* cross-sectional area $\mathscr{A}$ in momentum space of the Fermi surface cut by planes normal to the field $H$, the constant of proportionality involving only universal constants. The relation is

$$\Delta(1/H) = eh/c\mathscr{A}, \tag{2}$$†

and it can easily be shown that (2) reduces, as it should, to (1) for the special case of ellipsoidal energy surfaces. In general, there may be several closed regions of the Fermi surface which are relevant, and we should then expect each to contribute its own oscillatory component with its own period. As we shall see later, there are in fact several oscillatory components present in each experimental curve. The theory for energy surfaces of arbitrary shape has been worked out in more detail by Lifshitz & Kosevich (1954, 1955), and the physical principles involved have been discussed by Pippard (1955).

By studying in detail the dependence of the periods of the de Haas–van Alphen oscillations in a metal on the orientation of the field with respect to the crystal axes, it should therefore be possible, using equation (2), to determine $\mathscr{A}(\xi)$ for all directions $\xi$, and hence to deduce the shape and size of the Fermi surface. This can be done, under certain restrictions, using an elegant geometrical theorem recently given by Lifshitz & Pogorelov (1954). Comparison of equation (2) with the results of experiments in moderate fields (of order 15 kG) shows at once that the values of $\mathscr{A}$ are much smaller than would be expected from the main part of the Fermi surface of a metal. Thus the oscillations observable in moderate fields presumably arise from only small parts of the Fermi surface—small 'pockets' either of electrons at places where the surface overlaps a Brillouin zone boundary, or of positive holes left inside a nearly full zone. It is therefore only the shape of the surface round such pockets which can be obtained from experiments in moderate fields.

This paper describes a detailed investigation of the orientation dependence of the de Haas–van Alphen effect in aluminium at fields up to 15 kG with the view to trying out the practical applicability of the above method of studying the Fermi surface. Aluminium was chosen because (*a*) it has not proved possible to interpret its behaviour in terms of ellipsoidal energy surfaces, (*b*) it has cubic symmetry, thus making the interpretation somewhat simpler than for a metal of lower symmetry, and (*c*) the oscillations contain a component whose period is one of the lowest exhibited by any metal and which therefore

* In practice the extremum is usually a maximum, and we shall, in what follows, assume that a maximum is implied.

† Since this was written I have learnt that the same result was obtained independently by I. M. Lifshitz and reported to a meeting of the Ukrainian Academy of Sciences in January 1951.



PHILOSOPHICAL TRANSACTIONS OF THE ROYAL SOCIETY A MATHEMATICAL, PHYSICAL & ENGINEERING SCIENCES

arises from relatively large parts of the Fermi surface. The method of experiment adopted has been to study the torque on a single crystal by means of an improved form of the torsion apparatus used by Shoenberg (1952). The variation of torque with field has been measured for many different orientations of the field relative to the crystal axes, and from a detailed analysis of the dependence of periods on field direction it has indeed proved possible to deduce the shape and size of the relevant parts of the Fermi surface. The main emphasis throughout has been on the determination of periods, but some results on the temperature-dependence of amplitudes, and on the influence of adding small amounts of magnesium to aluminium have also been obtained; their relevance will be discussed at the end of the paper.

## 2. Experimental details

### (*a*) *The torque meter apparatus*

The conventional method of studying the de Haas–van Alphen effect is to measure the torque exerted on a single crystal of the metal in a uniform magnetic field. The crystal is attached to the bottom of a long quartz rod suspended by a short torsion wire, and the torque is measured by observing the deflexion of a beam of light reflected from a mirror on

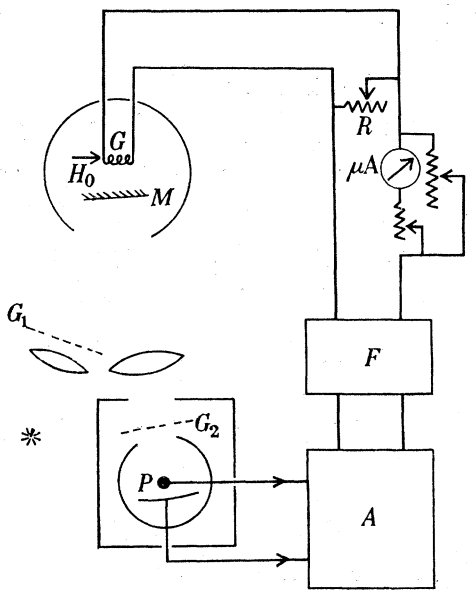


Figure 1. Schematic diagram of torque meter. $G$, galvanometer coil; $M$, mirror attached to suspension; $H_0$, magnetic field produced by permanent magnet; $P$, photocell; $A$, thyratron amplifier; $F$, smoothing filter; $G_1$, $G_2$, vertical grids.

the suspension. A difficulty of the method is that if, as for aluminium, the phase of the oscillations is sensitive to the orientation of the field, the movement of the crystal caused by the twisting of the suspension can cause distortions of the de Haas–van Alphen curves, and may even produce positions of instability (Shoenberg 1952). The apparatus has therefore been modified to reduce the angular motion of the crystal without loss of sensitivity by introducing an electrical feed-back device (cf. Croft, Donahoe & Love 1955).

The device is illustrated schematically in figure 1. Light from the mirror $M$ on the suspension falls on the photocell $P$, the output current of which is amplified by the thyratron

amplifier $A$, smoothed by the filter $F$, backed off by a suitable constant current and finally fed back into the galvanometer coil $G$ attached to the suspension and surrounded by a small permanent magnet. The torque on the coil opposes the torque on the crystal, and reduces the deflexion to a value much smaller than it would have had in the absence of feed-back; the current in the coil is then proportional to the torque on the crystal and provides a convenient measure of it. The sensitivity of torque measurement (i.e. meter reading per unit torque) is controlled by the shunt resistance $R$ across the coil, while variation of the amplification of $A$ controls the twist of the crystal per unit torque. The stiffness of the phosphor bronze fibre used ($\sim 75$ dyn cm/rad) is unimportant, since by increasing the amplification the final twist can be made arbitrarily small. To remove any self-sustained oscillations of the system ('hunting'), damping was provided by immersing two vanes attached to the upper end of the suspension in oil. In order to get a large change of light on the photocell for a small change in deflexion, vertical grids $G_1$ and $G_2$ were placed over the light source and over the photocell window so that the image of $G_1$ coincided with $G_2$. The sensitivity of the apparatus for $R = \infty$ was about 50 $\mu$A/dyn cm, but suitable adjustment of $R$ and $A$ made it possible to measure accurately torques anywhere in the range 0·002 to 20 dyn cm without the twist of the crystal exceeding 0·1° (which was not large enough to distort the de Haas–van Alphen oscillations).

### (*b*) *The magnetic field*

A Weiss electromagnet was used, capable of producing 15·4 kG in a 5 cm pole gap at about 100 A. This field was stabilized to about 0·05 % against fluctuations of longer than 0·1 s duration by means of a single feed-back loop electronic stabilizer. The potential difference across a very low resistance in the magnet circuit was balanced against a pre-set voltage tapping from a neon voltage regulator tube, and the difference amplified and used to control the field of a short-response-time variable motor-generator set (Amplidyne). The output of the Amplidyne was fed into the field windings of the main 30 kW generator supplying the magnet, so that the voltage tapping from the neon, in this way, controlled the magnetic field. The magnet was calibrated by the conventional flip coil and fluxmeter method, and the slope of the curve of field against current was determined to about $\frac{1}{4}$ % over the range of 8 to 15·4 kG, though the absolute field values were probably subject to inaccuracies of as much as 1 %. The field was homogeneous to about 1 part in $10^3$ over a region of 8 mm on either side of the centre of the magnet pole gap.

### (*c*) *The specimens*

All the pure aluminium crystals were grown in the form of rods about 4 mm long and 1·9 mm in diameter from spectroscopically pure material (Johnson, Matthey Lab no. 5941 X). They were prepared by solidification from the melt in a vacuum by means of a slow-travelling furnace. The crystals of aluminium containing magnesium were grown by the method of strain anneal, since a solidifying boundary advancing along a rod of molten alloy would probably result in lengthwise magnesium-rich streaks.

Each crystal was mounted on a short copper wire, weak enough to allow the orientation to be altered by bending the wire, but stiff enough to retain that orientation during the measurements. One end of the wire was attached to the long quartz suspension rod, and

the etched crystal was joined to the other end by indium soldering on to a small section of the aluminium which previously had been lightly electroplated with copper. By bending the wire while the quartz rod was mounted on an optical goniometer table, it was possible to set the crystal to any desired orientation with an accuracy of about 3°. Orientation errors arising from transferring the crystal from the goniometer to the freely hanging suspension were found to be almost negligible with this method of mounting, and, moreover, it was not necessary to remount the crystal for each new orientation. Immediately before bending the copper wire into a new direction, the preceding orientation of the crystal was usually checked on the goniometer in order to confirm that it had been retained during the low-temperature measurements.

To determine accurately the angular position of the projection of a tetrad axis in the horizontal plane when the suspension was hanging freely in the pole gap, a plot of torque against horizontal magnet rotation angle at a constant field of 14·6 kG at 4·2° K was made at the beginning of each helium run. The magnet rotation angle at which the plotted curve has a position of inverted mirror symmetry then fixed the direction of the projection of a tetrad axis in the horizontal plane to about 0·1° (Shoenberg 1952). The angle which the tetrad axis makes with the horizontal plane is, however, still subject to the uncertainty of about 3° arising from the goniometer measurements.

## 3. Period anisotropy of the high-frequency oscillations

### (*a*) *Experimental procedure and results*

The experimental procedure was to choose a temperature in the range 1·1 to 4·2° K such that the amplitude of the oscillations being studied was conveniently large, and then to tabulate galvanometer feed-back current (i.e. torque) against magnet current for the magnet current range 68 to 100 A. Readings were taken at magnet current intervals close enough (usually $\frac{1}{6}$ A) to yield about seven torque readings per cycle of the highest frequency oscillations present. In order to investigate the dependence of the periods on the orientation of the field, these tabulations were carried out for numerous field directions in a number of specially chosen crystallographic planes, the orientation in each plane being defined by the angle $\psi$ which $H$ makes with the projection of a tetrad axis in that plane. To change to a new horizontal plane of rotation of $H$, it was necessary to re-orientate the crystal on its mounting. Each of these tabulations of torque against magnet current was then plotted graphically as a curve of torque against $1/H$ by means of the known field calibration of the magnet. Automatic recording methods could not be used because a small change in field was found to produce transient torques through the eddy currents induced in the crystal, which, in aluminium in particular, were much larger than the steady de Haas–van Alphen torques being measured; thus the necessity of at least a 10 s wait after each increase of field made automatic recording impracticable.

Some typical de Haas–van Alphen curves are shown in figures 2 to 5. It can be seen that the curves contain 'low-frequency' oscillations (periods $\Delta(1/H)$ from 15 to $37 \times 10^{-7}$ G$^{-1}$) on which are superimposed 'high-frequency' oscillations (periods from 1·7 to $3{\cdot}6 \times 10^{-7}$ G$^{-1}$); both low and high frequencies often show beats, indicating that each group of oscillations contains several periodic terms of somewhat different periods. Since it proved difficult to

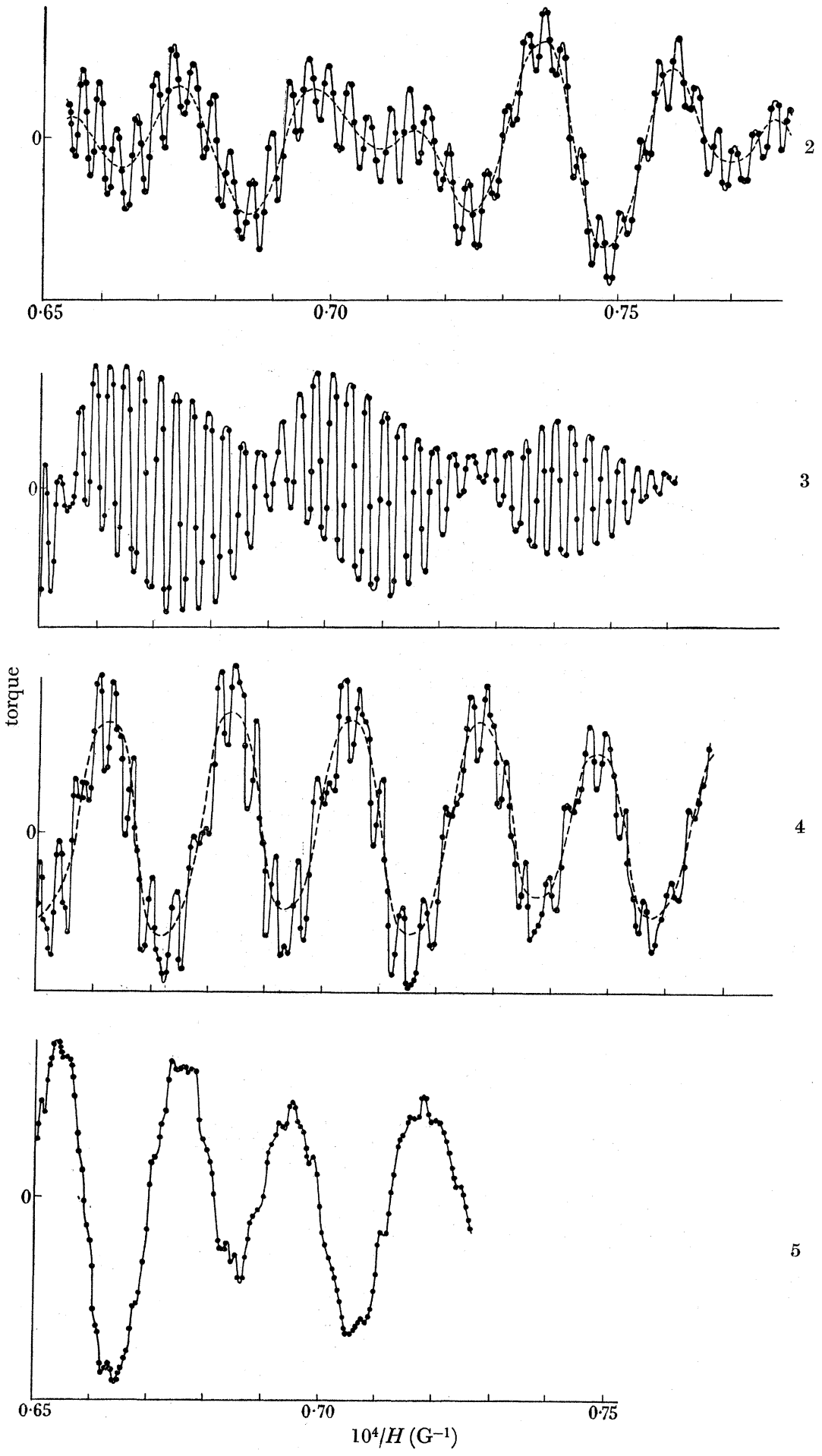




PHILOSOPHICAL TRANSACTIONS OF THE ROYAL SOCIETY A MATHEMATICAL, PHYSICAL & ENGINEERING SCIENCES

analyze the low-frequency oscillations reliably into separate periodic terms (because the field sweeps could not be made long enough to cover enough beats), most of the discussion which follows will be concerned only with the high-frequency oscillations, and the low-frequency oscillations will be briefly discussed later (§ 4*a*). Figure 2 shows a curve in which only one high-frequency term has appreciable amplitude, figure 3 shows a curve having beats between two high-frequency terms of nearly equal periods, but which contains relatively little low-frequency component, figure 4 is an example of a curve containing two high-frequency terms whose periods are rather different, and figure 5 is an example of a curve in which two high-frequency terms are detectable, but both of very small amplitude compared with the low-frequency terms.

Although the plotted de Haas–van Alphen curves contain about seven points per cycle of the high-frequency oscillations, they are nevertheless not of sufficient quality to warrant an accurate Fourier analysis, the amplitudes being too uncertain and the field sweeps not always long enough to allow the beat patterns to repeat themselves. The analysis of the curves of torque against $1/H$ into their composite high-frequency periods was therefore carried out by the following, somewhat more empirical, but simpler methods.

If only one high-frequency oscillatory term has appreciable amplitude (as in figure 2), the determination of its period presents no difficulty; as many periods as possible are counted and the range of $1/H$ they occupy divided by the number counted gives the required period.* If two high-frequency terms are present with nearly equal periods but with appreciably different amplitudes (as in figure 3), beats occur, but the individual oscillations can still be followed at the beat waists. If the procedure for a single frequency is now applied over a range covering several beats, the period obtained is that of the term of larger amplitude. The other period is then determined in an obvious way from measurement of the beat period. If, however, the amplitudes are very nearly equal, the extrema of the oscillations disappear at a beat waist; the procedure for a single frequency, if applied over several beats, now gives the harmonic mean of the two periods. If there are two high-frequency periods whose values differ considerably, so that only two or three oscillations are present in each beat period (as in figure 4), then a quick though rough method if the upper period has the dominant amplitude, is to estimate the upper period by counting only the large amplitude high-frequency peaks, and the lower period by counting all high-frequency peaks. Figure 5 is an example of a curve in which the high-frequency amplitudes are much smaller, but

* For this purpose periods may be taken to mean intervals between successive maxima (or minima); strictly speaking, zeros rather than extrema should be used since the periodic curve is modulated, but the modulation is gradual enough to make this error negligible.

---

FIGURE 2. de Haas–van Alphen curve exhibiting one high-frequency term; (100) plane. $\psi = 25{\cdot}0°$; $T = 1{\cdot}27°\,\mathrm{K}$; – – – – indicates low-frequency component.

FIGURE 3. de Haas–van Alphen curve exhibiting two high-frequency terms of nearly equal periods; (110) plane. $\psi = 50{\cdot}0°$; $T = 2{\cdot}77°\,\mathrm{K}$.

FIGURE 4. de Haas–van Alphen curve exhibiting two high-frequency terms whose periods differ considerably; (110) plane. $\psi = 86{\cdot}0°$; $T = 2{\cdot}77°\,\mathrm{K}$; – – – – indicates low-frequency component.

FIGURE 5. de Haas–van Alphen curve exhibiting two high-frequency terms with small amplitudes; (100) plane. $\psi = 42{\cdot}5°$; $T = 2{\cdot}57°\,\mathrm{K}$.

where the method just mentioned can still be applied; it illustrates the difficulty of reliable analysis for small amplitudes.

As will be explained in § 3 (*b*), it later became necessary to look for more than two high-frequency terms, and several curves were indeed found whose high-frequency oscillations could not be satisfactorily accounted for by two components alone. Figure 6 shows one such

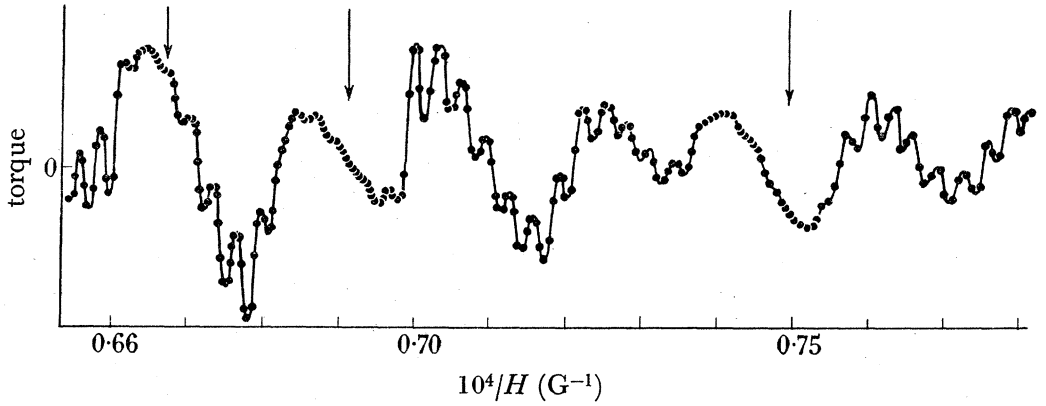


FIGURE 6. de Haas–van Alphen curve exhibiting three high-frequency terms. $H$ is in the direction $\psi = 65{\cdot}0°$ in a plane obtained from a (110) plane by tipping a [110] direction up by $7\frac{3}{4}°$; $T = 1{\cdot}32°$ K. Vertical arrows indicate approximate positions of zero beat waists. The periods deduced from the curve were 3·10, 2·78 and $2{\cdot}70 \times 10^{-7}$ G$^{-1}$

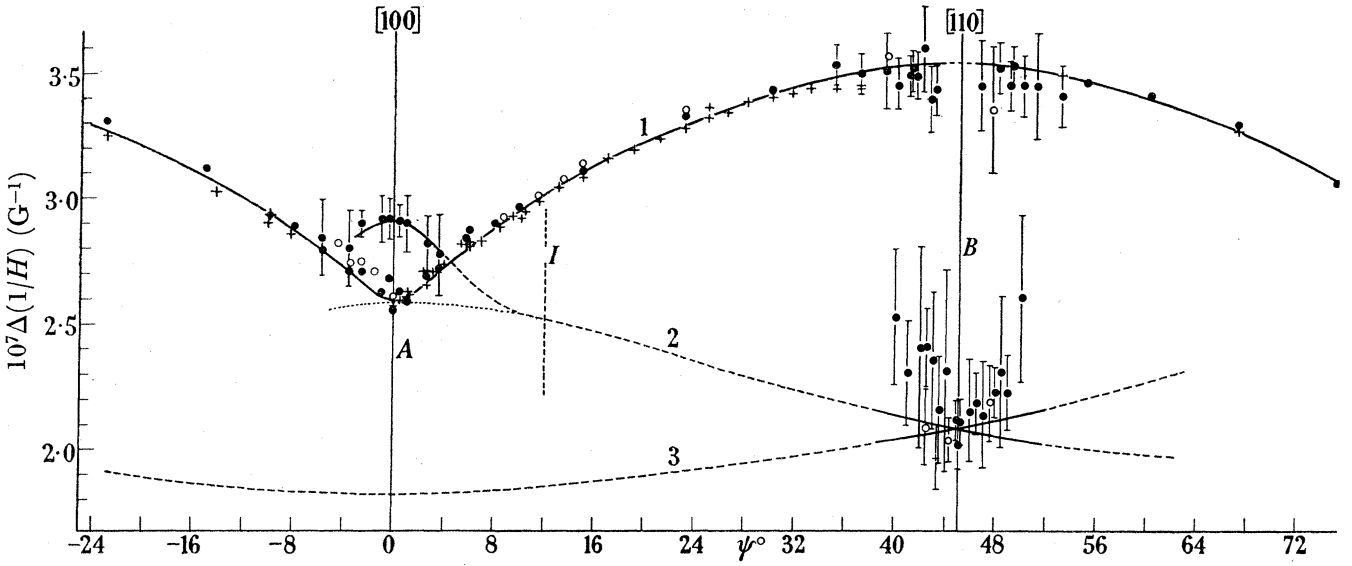


FIGURE 7. Variation of high-frequency periods with $\psi$ in a (100) plane.
The various kinds of points refer to the various crystal specimens.

example, and it can be seen that beat waists of approximately zero amplitude occur at quite unequal intervals. This is characteristic of a curve made up of three periodic terms in which two of the periods are nearly equal and the third is rather different; the separate periods were estimated from detailed considerations of the manner in which the amplitude fluctuated.

In some cases trial synthesis greatly assisted the analysis as well as providing a useful check; sinusoidal terms of the appropriate frequencies were added, and their relative amplitudes adjusted until the experimental curves (from which the low-frequency component had first been subtracted) were sufficiently closely reproduced. These syntheses were done graphically at first, but later an electrical method was developed in which the outputs from three beat-frequency oscillators were superimposed and displayed on an oscilloscope screen.

The chosen crystallographic planes which were set horizontal, and in which $H$ was rotated, were a (100) plane, a (110) plane, a (111) plane, the plane obtained from a (100) plane by tipping one tetrad axis up by $12\frac{1}{2}°$, and the plane obtained from a (110) plane by tipping a [110] direction up by $7\frac{3}{4}°$. The variation of high-frequency period with $\psi$ obtained in each of these planes is shown in figures 7 to 11; the reasons for joining up the experimental

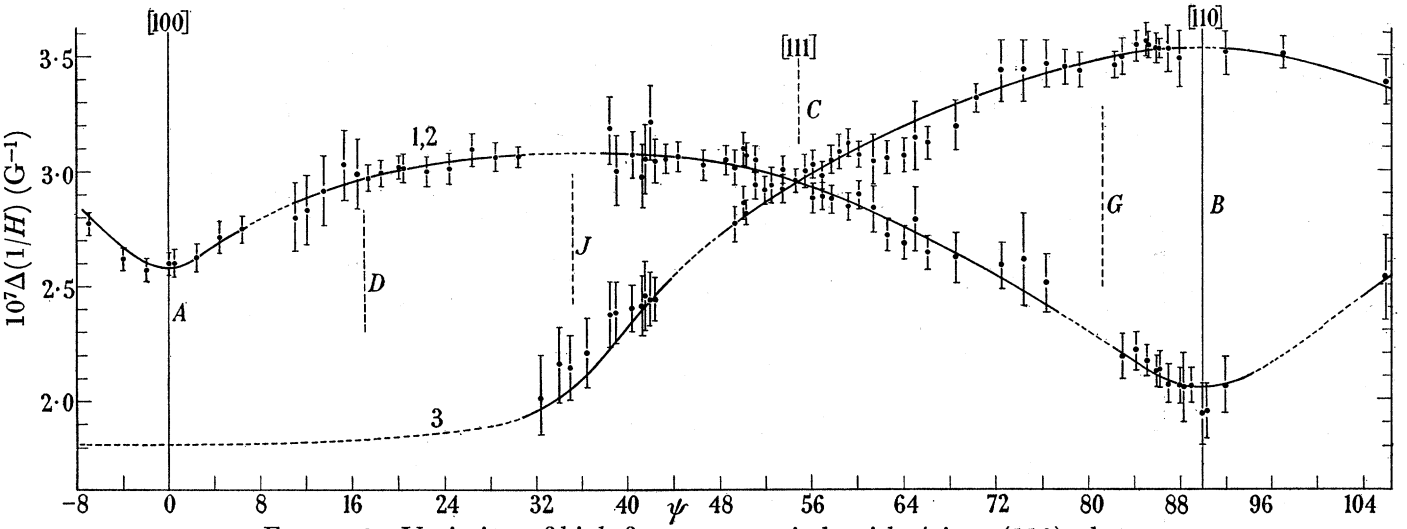


FIGURE 8. Variation of high-frequency periods with $\psi$ in a (110) plane.

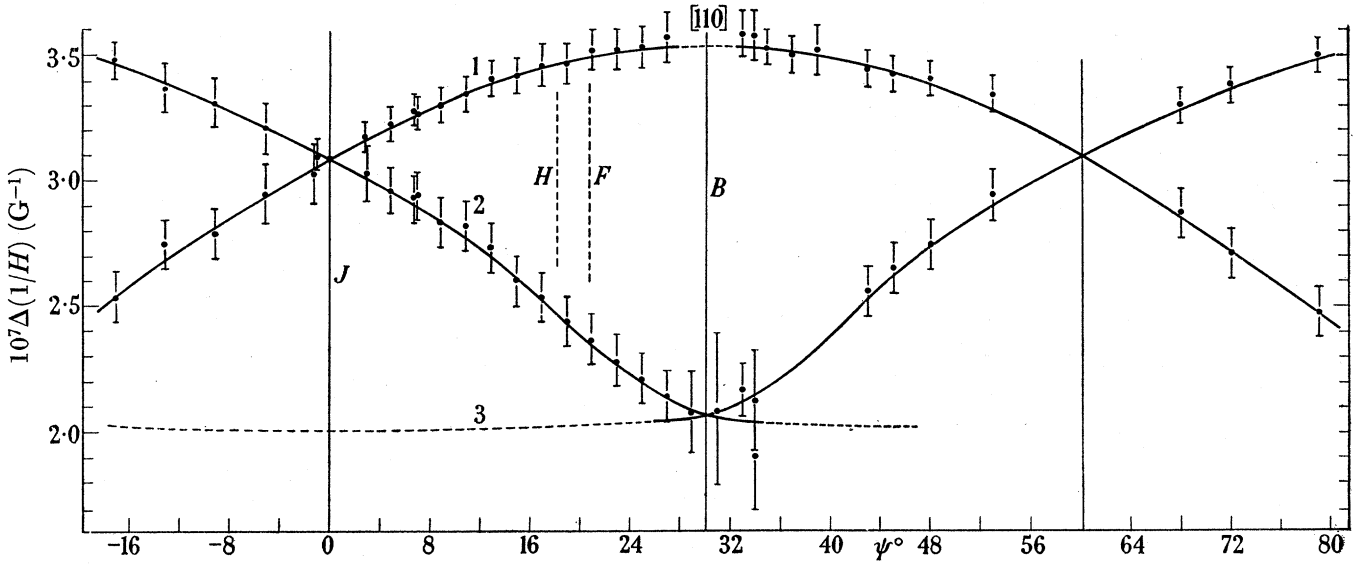


FIGURE 9. Variation of high-frequency periods with $\psi$ in a (111) plane.
At $J$ oscillations having no beats were observed.

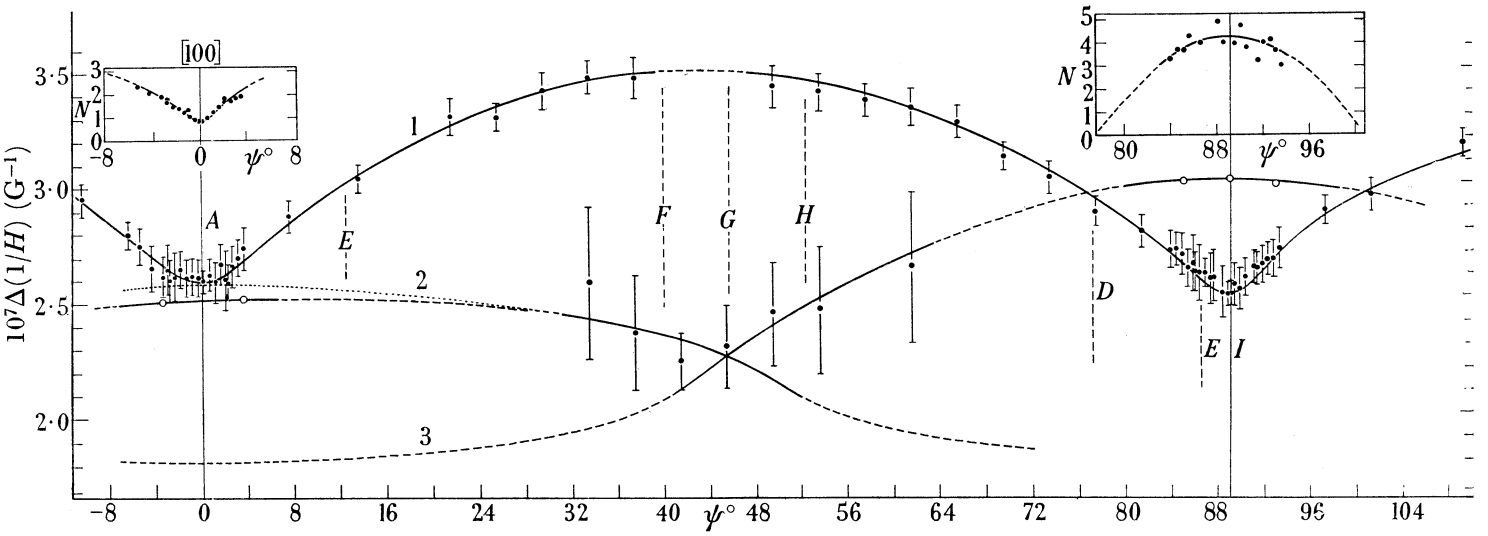


FIGURE 10. Variation of high-frequency periods with $\psi$ in a plane obtained from a (100) plane by tipping one tetrad axis up by $12\frac{1}{2}°$. The two insets are plots of the number of beats $N$ in the interval from 0·65 to 0·725 of $10^4/H$. The points ○ are periods deduced from the smoothed graphs of $N$.

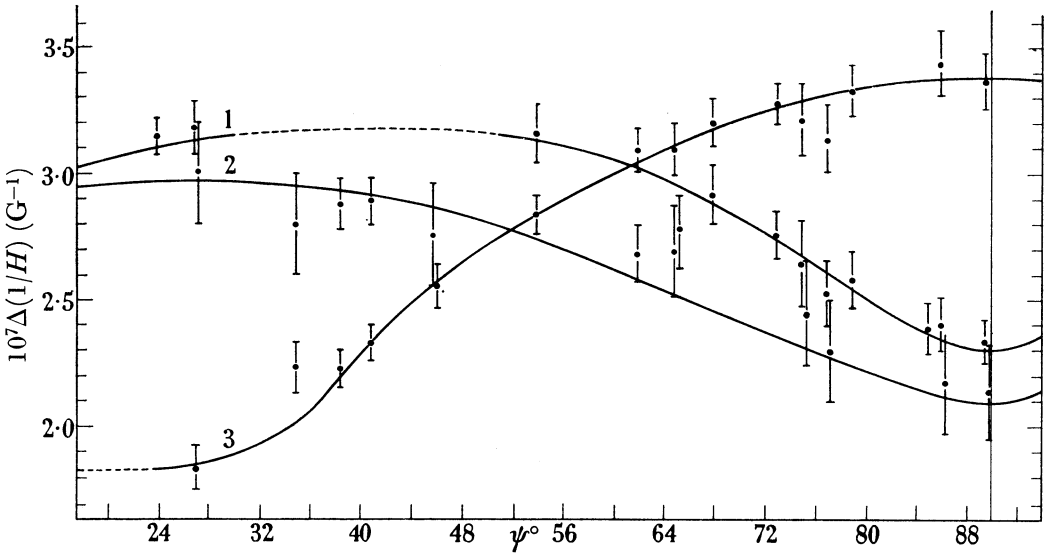


FIGURE 11. Variation of high-frequency periods with $\psi$ in a plane obtained from a (110) plane by tipping a [110] direction up by $7\frac{3}{4}°$. Where three periods occur simultaneously, one of the corresponding points has been slightly displaced laterally to avoid confusion.

points by the curves shown will be discussed below (§ 3(*b*)). The high-frequency periods for any one crystal were found to be reproducible to about 2% from run to run. The reproducibility from one crystal to another, however, was rather poorer, but this could be accounted for by small errors in orientation. For instance, sometimes beats between two high-frequency terms occurred for the field direction near a [100] axis in what was nominally a (100) plane, and sometimes not, depending on how accurately the (100) plane was coincident with the plane of rotation of the field. As will be explained in § 4(*b*), the frequent occurrence of gaps in the curves of period against $\psi$ is probably due to the amplitudes of those high-frequency terms becoming undetectably small.

*(b) Interpretation of the anisotropy of the high-frequency periods*

Nearly all of the de Haas–van Alphen curves used in the four sweeps of figures 7 to 10 were found to be interpretable in terms of only two high-frequency components, but occasionally an anomalous beat pattern was observed which did not appear to be explicable by less than three high-frequency components of different periods (e.g. figure 6). Moreover, in devising a scheme of period values for all directions in space, which would interpolate satisfactorily and consistently between the sets of directions represented in figures 7 to 10, and which would indicate how to bridge the gaps between the plotted points in this diagram, it was found necessary to assume that three oscillatory components were present at each orientation, but that one of them was usually undetectable because of its low amplitude. For instance, the field direction represented by $J$ on the period-$\psi$ variation in the (111) plane (figure 9) also occurs at $\psi = 35°$ in the (110) plane (figure 8). Figure 9 shows that for this field direction there are two coincident periods with $\Delta(1/H) = 3{\cdot}09 \times 10^{-7}\,\mathrm{G}^{-1}$, while figure 8 shows an additional period of $2{\cdot}04 \times 10^{-7}\,\mathrm{G}^{-1}$. Although only the $2{\cdot}04 \times 10^{-7}\,\mathrm{G}^{-1}$ period occurs at $J$ in figure 8, the upper curve (marked 1, 2), drawn to bridge the gap at $J$, does pass through just the correct value, $3{\cdot}09 \times 10^{-7}\,\mathrm{G}^{-1}$ at $\psi = 35°$ (i.e. the value that corresponds to $J$ in figure 9). We see then that in this case, the assumption of three, rather than two, components is unavoidable. The fact that quite different relative amplitudes of the three components occur in different sweeps for the same direction of the field relative to the crystal axes (e.g. $J$ in figures 8 and 9) is due to the fact that the axis of measurement of torque is different in the different sweeps (see §4 (*b*)).

This interpretation implies that in the sweep in the (110) plane there are two terms of coincident period, but of negligible amplitude at the orientation $J$; the symmetry arguments given below indicate even more, namely, that the two terms should have identical periods not only at $J$, but along the whole of the curve marked 1, 2 in figure 8. If, however, the sweep plane is slightly different from (110), these two periods corresponding to the single curve 1, 2 in figure 8 should become slightly different, and it should then be possible to observe three periods simultaneously. It was for this reason that the sweep of figure 11, in a plane obtained from a (110) plane by tipping a [110] direction up by $7\frac{3}{4}°$, was made, and it can be seen that the 1, 2 curve has indeed split up as expected. As mentioned in the previous section, curves exhibiting three high-frequency terms were indeed found in this plane; figure 6 shows one such example.

Once it was clear that there were three high-frequency terms present, it became possible to draw the mutually consistent curves shown in figures 7 to 11 through the experimental points. The parts of the curves not covered by experimental points are indicated by dashed lines, and it will be realized, of course, that these dashed curves are somewhat schematic, particularly in the regions of low period close to the tetrad axes.

The dotted curves in figures 7 and 10 indicate how the periods would behave if the orientations were exactly correct. For instance, in figure 10, one of the tetrad axes (projection on plane of rotation of $H$ indicated by $I$) was deliberately tipped up by $12\frac{1}{2}°$, but it was found on checking the orientation after the sweep had been completed that the other tetrad axis (projection indicated by $A$) had inadvertently been tipped down by $5\frac{1}{2}°$. The curves in figure 7 around $\psi = 45°$ have been drawn to join up as smoothly as possible with

the rest of the diagram. The experimental points in this region tend to lie systematically above the drawn curves; this is probably because the method of period analysis becomes unreliable when, as here, the amplitude of the upper-period term obscures that of the lower-period terms. The indicated uncertainties of some of the experimental points have in fact probably been underestimated.

So far the scheme of joining up the experimental points of figures 7 to 11 has been presented mainly from an empirical point of view; it is, however, strongly supported by the following symmetry considerations, which, indeed, suggested the scheme in the first place. Aluminium has a face-centred cubic lattice, and the reduced Brillouin zone of such a lattice is illustrated in standard texts (e.g. Mott & Jones 1936, p. 157). The small parts of the Fermi surface responsible for the high-frequency oscillations are likely to be situated close to various points of symmetry in the Brillouin zone. If, for instance, they are centred on the twenty-four corner points $W$ of the zone, the twenty-four pieces of surface can be joined together to give three pairs of closed surfaces. The two members of each pair are inversion images of one another, which implies that they give rise to equal de Haas–van Alphen periods for any orientation of the magnetic field. The variation of the period with orientation due to any one pair of surfaces has the fourfold symmetry of a cushion (point group $4/mmm$), and the fourfold axes of the three pairs lie along the three tetrad axes of the face-centred cubic lattice. The pattern of the variation with orientation of the periods due to these three pairs of surfaces, or 'pockets', as we shall call them subsequently, would show, among others, the following features:

(1) there would be in general three, and only three, periods for any one orientation of the field;

(2) in a (100) plane one period would have fourfold rotational symmetry and the other two periods twofold rotational symmetry;

(3) in a (110) plane two of the periods would coincide for all angles $\psi$, and all three periods would be equal for the field along a [111] direction ($C$ in figure 8);

(4) in a (111) plane each of the three periods would have twofold rotational symmetry.

These features would be shown also if the pieces of Fermi surface were situated round the centres $X$ of the square faces, but not at any other points on the zone. The observed patterns (figures 7 to 11) are indeed consistent with all these features, though in view of the 'gaps' due to insufficient amplitude, it is of course impossible to be quite sure. We conclude, therefore, that the pieces of the Fermi surface giving rise to the high-frequency oscillations are centred round the points $W$ or $X$ in the Brillouin zone; later (§ 3 ($d$)) reasons will be mentioned for assigning them to $W$ rather than $X$.

### (c) *Representation of the period anisotropy results on a stereographic plot*

In order to carry out the calculation of the shape of the Fermi surface, it is necessary to know the high-frequency periods for any arbitrary orientation of $H$; i.e. to interpolate period values for orientations intermediate between those covered by figures 7 to 11. This can most conveniently be done by representing $H$ directions as points on a stereographic projection and then constructing contour lines of equal period on this projection. A separate stereographic contour diagram has to be drawn for each of the three periods marked as 1, 2 and 3 in figures 7 to 11, since each arises from a different pocket (or from a different

pair of symmetrical pockets) of the Fermi surface. Because these three pockets must, to satisfy the zone symmetry, be inclined mutually at right angles, these three contour diagrams differ from each other only by 90° rotations. If the three contour diagrams are superimposed, the three high-frequency periods observed in practice can be read off at any orientation. Owing to the cubic symmetry of the triple-valued contour diagram, contours for the three periods need only be drawn in one of the elementary triangles bounded by (100) and (110) planes (i.e. in $\frac{1}{48}$th of the solid angle $4\pi$ of all $H$ directions). But if all the information is to

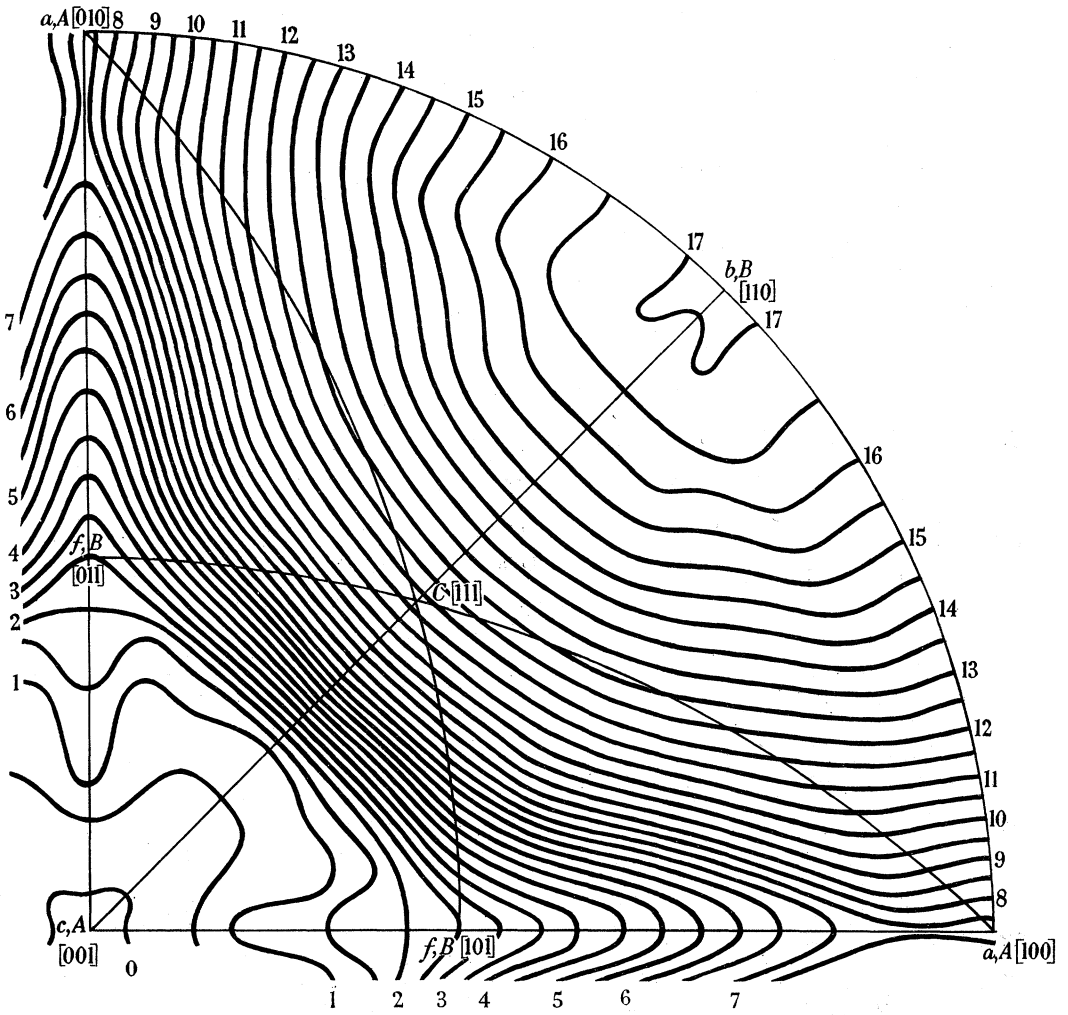


FIGURE 12. Contour diagram of period $\Delta(1/H)$ of the high-frequency oscillations represented by the curves of figures 7 to 11 over one octant of a stereographic projection. The fourfold axis is at the centre of the projection for period 3. Alternate contours are numbered: contour no. 0 corresponds to $\Delta(1/H) = 1{\cdot}83 \times 10^{-7}$ G$^{-1}$ and no. 17 to $\Delta(1/H) = 3{\cdot}53 \times 10^{-7}$ G$^{-1}$; the contour spacing is $0{\cdot}05 \times 10^{-7}$ (i.e. $0{\cdot}1 \times 10^{-7}$ between successive numbered contours). The various letters correspond to directions marked in figures 7 to 10 and 13.

be displayed on a single-valued contour diagram corresponding to one of the Fermi surface pockets, then contours in $\frac{1}{16}$th of the stereographic projection must be drawn. Figure 12 shows a contour diagram for one of the pockets, for one octant of the solid angle $4\pi$ of $H$ directions, the relevant period being period 3. For periods 1 and 2, the contour diagrams would have their fourfold axes at the pole or at the equatorial extreme respectively.

To check the reliability of the contours, additional period measurements were made for several $\psi$ values in a plane chosen to pass approximately through the centre of an elementary triangle; these measurements were made with about 1 % accuracy by using especially long field sweeps. As can be seen from table 1, the period values obtained agree to within 2 % with those read off the contour diagram. A further check on the consistency of the contour diagram comes from the observation that at the orientations where the planes of rotation of $H$ used in figures 7 to 11 intersect, the periods measured experimentally in each plane

TABLE 1. A CHECK ON THE RELIABILITY OF THE CONTOUR DIAGRAM (FIGURE 12)

| | | $10^7\Delta(1/H)$ ($G^{-1}$) | |
|---|---|---|---|
| $\psi°$ | $T°K$ | measured | read directly off figure 12 |
| 10·0 | 2·07 | 2·92, 2·73 | 2·90, 2·74 |
| 17·0 | 2·07 | 3·09 | 3·08 |
| 24·0 | 2·07 | 3·24 | 3·22 |
| 31·0 | 2·07 | 3·30, 2·83 | 3·30, 2·80 |
| 59·0 | 1·98 | 2·97 | 2·95 |
| 66·0 | 1·99 | 3·10 | 3·08 |
| 73·0 | 1·98 | 3·21, 2·90 | 3·21, 2·93 |
| 82·0 | 1·88 | 2·56 | 2·58 |
| 90·0 | 1·84 | 2·35 | 2·31 |

agree with each other to within about 2 % (such points are marked by corresponding letters in the various diagrams). The contours are thus probably accurate to within half a contour spacing everywhere except in the immediate vicinity of the fourfold axis, where no experimental values exist at all and where the contours are only schematic (as are, of course, the corresponding parts of the sweep curves in figures 7 to 11).

### (*d*) *Calculation of the shape and size of the Fermi surface causing the high-frequency oscillations*

The problem of calculating the shape and size of the Fermi surface pockets causing the high-frequency oscillations is essentially that of determining a surface from a knowledge of its maximum cross-sectional area $\mathscr{A}(\boldsymbol{\xi})$ in planes normal to a unit vector $\boldsymbol{\xi}$ for all directions $\boldsymbol{\xi}$. However, $\mathscr{A}(\boldsymbol{\xi})$ does not determine the shape of the surface uniquely unless it is assumed that the surface has a centre of symmetry and that the surfaces are not too contorted. Under these assumptions the cross-section of maximum area perpendicular to a particular direction is always a central cross-section. Since the pieces of the Fermi surface, if centred about the points $W$ on the Brillouin zone, would not have a centre of symmetry, the best that can be done in the way of determining their shape is to calculate the shape of the centro-symmetrical surface which has the same $\mathscr{A}(\boldsymbol{\xi})$ for all $\boldsymbol{\xi}$ as each of the actual pockets. This then represents a kind of average shape of the two members of the pair. An elegant solution of the mathematical problem for a centro-symmetrical surface has recently been given by Lifshitz & Pogorelov (1954). They find that the radius vector $\rho(\mathbf{e})$ of the surface in the direction of the unit vector $\mathbf{e}$ may be expressed as

$$\pi\rho^2(\mathbf{e}) = \chi_e(0) - \int_0^1 \{\chi_e(u) - \chi_e(0)\}\,\mathrm{d}u/u^2, \tag{3}$$

where

$$\chi_e(u) = \frac{1}{2\pi}\int_0^{2\pi} \mathscr{A}(\boldsymbol{\xi})\,\mathrm{d}\phi, \tag{4}$$

i.e. $\chi_e(u)$ is an average of $\mathscr{A}(\boldsymbol{\xi})$ taken round the latitude $\theta$. Here $u = \cos\theta$, $\theta$ is the angle between the unit vectors $\boldsymbol{\xi}$ and $\mathbf{e}$, and $\phi$ is the corresponding azimuthal angle (note that $u = (\mathbf{e}.\boldsymbol{\xi})$); if $\boldsymbol{\xi}$ is the direction of the field, then $\mathscr{A}(\boldsymbol{\xi})$ is related to the period $\Delta(1/H)$ by equation (2).

This leads to the following practical procedure for calculating $\rho(\mathbf{e})$. First $\chi_e(u)$ is determined for a particular $\mathbf{e}$ by averaging the values of the reciprocal of the periods read from

TABLE 2. VALUES OF $\chi_e(u)$

$\chi_e(u) \times 9{\cdot}4 \times 10^{40}$*

| $\theta°$ | $u$ | $a$ | $b$ | $c$ | $d$ | $f$ |
|---|---|---|---|---|---|---|
| 90 | 0 | 46·92 | 41·01 | 31·57 | 41·97 | 36·25 |
| 87·5 | 0·044 | 46·46 | 40·95 | 31·53 | 41·97 | 36·45 |
| 85 | 0·087 | 45·82 | 41·01 | 31·51 | 41·98 | 36·60 |
| 82·5 | 0·131 | 44·86 | 40·95 | 31·69 | 42·03 | 36·86 |
| 80 | 0·174 | 44·00 | 41·01 | 31·96 | 42·03 | 37·17 |
| 77·5 | 0·217 | 43·13 | 41·10 | 32·34 | 42·19 | 37·52 |
| 75 | 0·259 | 42·50 | 41·26 | 32·71 | 42·44 | 37·94 |
| 70 | 0·343 | 41·08 | 41·52 | 33·64 | 42·85 | 38·68 |
| 65 | 0·423 | 39·65 | 42·12 | 34·83 | 42·40 | 39·04 |
| 60 | 0·500 | 38·24 | 42·83 | 36·03 | 40·73 | 38·99 |
| 55 | 0·575 | 36·95 | 42·52 | 37·52 | 38·99 | 38·83 |
| 50 | 0·643 | 35·77 | 41·13 | 39·58 | 37·47 | 38·90 |
| 40 | 0·768 | 34·28 | 35·95 | 45·90 | 35·53 | 39·68 |
| 30 | 0·867 | 34·12 | 32·40 | 51·70 | 34·21 | 40·90 |
| 20 | 0·942 | 34·65 | 29·96 | 52·21 | 32·00 | 42·88 |
| 10 | 0·987 | 35·82 | 28·71 | — | 30·50 | 45·64 |
| 0 | 1·000 | 39·10 | 28·10 | 54·40 | 30·00 | 48·10 |

* The figures given are actually the averages of $10^{-5}/\Delta(1/H)$ round each latitude $u = \cos\theta$; they are therefore values of $\chi$ multiplied by $(c/eh) \times 10^{-5}$, i.e. $9{\cdot}4 \times 10^{40}$.

TABLE 3. SUMMARY OF CALCULATION OF $\rho$ VALUES

| | $9{\cdot}4 \times 10^{40} \times$ | | | $10^{20}\rho$ | | |
|---|---|---|---|---|---|---|
| direction | $\chi(0)$ | $\int_0^1 \left\{\frac{\chi(0)-\chi(u)}{u^2}\right\} du$ | $\pi\rho^2$ | direct method | $\lambda-\delta$ method | $\lambda-\delta$ method, 3 extra contours |
| $a$ | 46·9 | 53·5 (8) | 100·4 | 1·84 (0·07) | 1·78 | 1·79 |
| $b$ | 41·1 | 1·6 (1) | 42·7 | 1·20 (0·02) | 1·23 | 1·26 |
| $c$ | 31·6 | −16·0 (2) | 15·6 | 0·73 (0·05) | 0·73 | 0·73 |
| $d$ | 42·0 | 3·9 (1) | 45·9 | 1·24 (0·01) | 1·23 | — |
| $f$ | 36·2 | −16·7 (5) | 19·5 | 0·81 (0·10) | 0·86 | — |

*Note.* The figures in brackets give rough estimates of the uncertainties arising in the evaluation of the integral from the range near $u = 0$, and the corresponding uncertainties in $\rho$.

the contour diagram at 2° intervals of $\phi$ round a particular latitude $\theta$. For any direction $\mathbf{e}$ represented by a point on the circumference of the contour diagram, the appropriate latitudes are defined as latitudes of a stereographic net whose pole is placed at the point representing $\mathbf{e}$. For other directions $\mathbf{e}$ it is simplest to draw a new counter diagram in which the plane of the projection contains $\mathbf{e}$, i.e. such that $\mathbf{e}$ is again represented by a point on the circumference. For each direction $\mathbf{e}$ a series of values of $\chi_e(u)$ for sufficiently closely spaced values of $u$ between 0 and 1 is obtained (see table 2), the integrand of (3) is plotted graphically, and the integration carried out by counting squares. The directions chosen for cal-

culation are shown in figure 13 and denoted by $a$, $b$, $c$, $d$, $f$; the calculation and the results for $\rho(\mathbf{e})$ are summarized in table 3.

Since $\chi_e(u)$ is an even function of $u$, $\{\chi_e(u)-\chi_e(0)\}/u^2$ should become independent of $u$ for sufficiently small values of $u$, i.e. the graph of the integrand in (3) should flatten out. In fact, however, the accuracy of determination of $\chi_e(u)$ becomes inadequate for $u$ less than about 0·1 and the 'flat' region is, for most directions $\mathbf{e}$, never well established, the graph appearing in some cases to continue steeply up, even at the smallest values of $u$. This makes the value of the integral in (3) uncertain by an amount which is difficult to estimate, though some indication of the uncertainty is given in table 3. It can be seen that the corresponding uncertainty in $\rho$ is not usually very serious. It is worst for $\rho(c)$ and $\rho(f)$ because the two terms in (3) then have opposite signs.

In order to avoid the uncertainty inherent in this direct method an alternative method was tried, based on an intermediate step in Lifshitz & Pogorelov's derivation of (3). This is

$$\pi\rho^2(\mathbf{e}) = \lim_{\lambda\to 0}\frac{2}{\lambda^2}\left\{\int_0^{\lambda}\chi_e(u)\,\mathrm{d}u-\int_{\lambda}^{1}\chi_e(u)\left(\frac{u}{(u^2-\lambda^2)^{\frac{1}{2}}}-1\right)\mathrm{d}u\right\}. \tag{5}$$

If the limit sign is omitted, the right-hand side of (5) can be calculated for a small finite value of $\lambda$ (0·1 was chosen), and this gives a value of $\rho$ averaged over a small range of directions around $\mathbf{e}$. This method is less sensitive to the uncertainties of the $\chi$ values near $u=0$ than is the 'direct' method, but, on the other hand, the answer it gives must involve some extra error because the limiting process in (5) has been omitted. The integrand of the second integral in (5) becomes infinite as $u\to\lambda$, and to avoid this infinity the range of integration is broken up into two parts: from $\lambda$ to $\delta$ where $\delta$ is still small ($\delta=0{\cdot}17$ was used, and it was shown that even for as high as $\delta=0{\cdot}25$ much the same answers were obtained), and from $\delta$ to 1. The first part is calculated analytically assuming $\chi(u)$ to vary linearly between $\lambda$ and $\delta$ (this can be shown to introduce negligible errors), and the second part graphically. The values for $\rho$ obtained by this '$\lambda-\delta$' procedure are also shown in table 3, and it can be seen that they agree quite well with the 'direct' values.

In the calculation of $\rho(\mathbf{e})$ by the direct method it can be seen that the most important contribution usually comes from $\chi_e(0)$; now since for directions $a$ and $b$ this involves the contours near the centre of the diagram, which, as has been explained in § 3 (*c*), are really only very roughly known, a check was made to see how the answers would be affected if the contour diagram were modified in this region. The lowest period was taken as $1{\cdot}68\times10^{-7}\,\mathrm{G}^{-1}$ instead of $1{\cdot}83\times10^{-7}\,\mathrm{G}^{-1}$, and three extra contours had to be accommodated. A recalculation of $\rho(a)$, $\rho(b)$ and $\rho(c)$ with the new contour diagram gave values very little different from the earlier ones (see table 3), so it is clear that the precise form of the lowest contours is not very significant for the final answers.

Taking into account the possibility that the contour diagram may be in error near the fourfold axis to an even greater extent than just suggested, and bearing in mind other errors that may have entered in the construction of the contour diagram, and also the computational errors and the various uncertainties explained above, it is probably safe to say that the $\rho$ values are reliable to better than 10%.

From the $\rho$ values it follows that the shape of each of the three 'pockets' of Fermi surface must be somewhat like that indicated by the cross-sections shown in figure 13; each of

the three calculated surfaces corresponds to a pair of non-centro-symmetric surfaces (cf. pp. 310, 312) and they have their principal axes mutually at right angles. The slight hump at $b$ shown in the section with fourfold symmetry ($ab$) is suggested by the fact that $\rho(d) \doteqdot \rho(b)$, but may not be real; the $ac$ section lies inside the ellipse determined by $\rho(a)$ and $\rho(c)$, since $\rho(f)$ is about 15 % less than would be appropriate for an ellipse with semi-axes $\rho(a)$, $\rho(c)$. As a check on the reliability of the shapes indicated, the areas of the cross-sections in the planes $ab$, $ac$ and $bc$ were estimated, treating the sections $ac$ and $bc$ as elliptical and $ab$ as a square of side $2\rho(b)$. These agreed reasonably with the reciprocal periods read off the contour diagram.

The volume of each pocket can be estimated roughly by treating the $ab$ section as a square of side $2\rho(b)$ and assuming that sections cut parallel to $b$ and normal to the plane $ab$ are elliptical of major semi-axis $\rho(b)$. This gives the volume as $v = \frac{1}{2}\pi^2\rho^2(b)\,\rho(c)$, or $5{\cdot}1 \times 10^{-60}\,\mathrm{g^3\,cm^3\,s^{-3}}$. The effective number of electrons (or positive holes) per atom for each pocket is $a^3v/2h^3$, where $a$ is the lattice spacing, and putting $a = 4{\cdot}04 \times 10^{-8}$ cm, we find $0{\cdot}6 \times 10^{-3}$ electron per atom. The total number is either 6 or 3 times as great, depending on whether the relevant pockets are situated at the points $W$ or $X$ on the zone.

The results just described throw some light on the question of whether $W$ or $X$ is the more probable location. Theoretical calculations by Heine (1957) on the expected form of the energy surface in aluminium show that pockets of positive holes where the Fermi distribu-

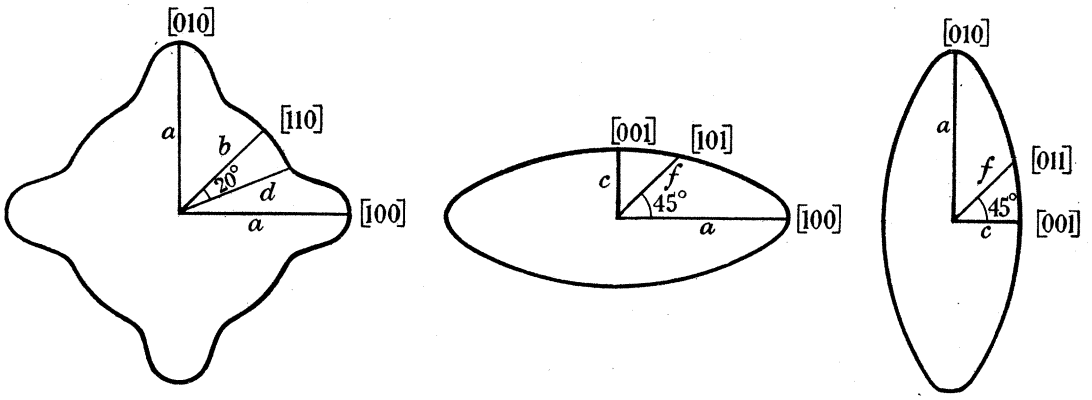


FIGURE 13. Plan and two elevations of one of the three cushion-shaped Fermi surface pockets. $a$, $b$, $c$, $d$, $f$ indicate the directions for which $\rho$ has been calculated.

tion just fails to fill the first Brillouin zone could have a shape consistent with that experimentally found if these pockets are located at $W$, but not if they are located at $X$ (pockets at $X$ would have the ratio of $\rho(a)$ to $\rho(c)$ much greater than that observed). These calculations have not been successful in identifying the still smaller pockets which are responsible for the low-frequency oscillations (see discussion in § 4 ($a$)).

## 4. MISCELLANEOUS EXPERIMENTAL RESULTS

### ($a$) *Period anisotropy of the low-frequency oscillations*

To determine the periods of the lower frequency terms it was necessary to measure torques at close field intervals over much longer field sweeps (9·5 to 15·4 kG) than those used in the high-frequency period measurements, since otherwise the beat patterns are too short

to permit reliable period analysis. Even with this maximum length of field sweep, reliable component periods for the lower-frequency terms were not always obtainable, and these lower-frequency periods have in fact been determined at only a few selected values of $\psi$ in a (100) plane. Table 4 gives the values obtained; most of these low-frequency measurements were taken at 4·2° K in order to reduce the relative amplitude of the high-frequency component. The low-frequency oscillations have only a single sinusoidal component near a [100] axis, but beats between two components occur for $\psi > 5°$; the separation of the two periods increases with $\psi$ and becomes greatest at $\psi = 45°$.

The data shown in table 4 are insufficient for building up any comprehensive picture of the overall dependence of low-frequency period on orientation, such as was obtained above for the high-frequency periods. Thus it has not proved possible to work out the shape of the pockets of Fermi surface responsible for the low-frequency oscillations. It might at first

TABLE 4. PERIOD VALUES OF THE LOW-FREQUENCY OSCILLATIONS IN A (100) PLANE

| $\psi°$ | $10^7\Delta(1/H)$ ($G^{-1}$) |
|---|---|
| 0·8 | 36·1 (0·3) |
| 1·2 | 37·2 (2·6) |
| 1·4 | 35·9 (0·2) |
| 6·0 | 37·1 (2·6) |
| 9·8 | 31·6* (2·5) |
| 16·2 | 36·3, 22·8 (4·0, 2·5) |
| 25·0 | 36·0, 24·0 (2·2, 1·9) |
| 30·2 | 19·95* (2·8) |
| 42·2 | 21·2* (2·9) |
| 44·0 | 36·1, 21·35 (3·2, 1·7) |

*Note.* The readings marked * showed evidence of a second period. The figures in brackets are rough estimates of the possible errors of the individual periods.

sight appear that the greater period, which appears to be independent of $\psi$, corresponds to a surface of revolution, but this interpretation is untenable since by symmetry such a surface would produce no torque. Evidently, more complete data are required about these low-frequency periods before the results can be unambiguously interpreted in terms of a Fermi surface shape. The effective number of free electrons (or positive holes) per atom contained in the pockets of the Fermi surface giving rise to the low-frequency periods must of course be considerably smaller than that giving rise to the high-frequency periods, and the sizes of the pockets must be correspondingly smaller.

### (*b*) *Anisotropy of the oscillation amplitudes*

Since absolute amplitude measurements proved to be rather irreproducible (for a discussion see Shoenberg (1952)), only qualitative information on the anisotropy of the amplitudes of the high-frequency terms could be obtained, and this is presented in figure 14. Lifshitz & Kosevich (1954, 1955) have developed Onsager's interpretation of the de Haas–van Alphen oscillations to give an explicit expression not only for the period but also for the amplitude of the oscillations, in terms of the geometrical features of energy surfaces of arbitrary form. In principle, comparison of these expressions with the data on absolute amplitudes could give additional information about the geometry of the energy surfaces, but actually the experimental data are too rough, and in any case other parameters may be relevant (e.g. broadening of the energy levels due to various causes (see Dingle 1952)) which would make the comparison of dubious value.

It is, however, worth noting some general principles which account qualitatively for some of the features of figure 14. First, the amplitude of each periodic term in the couple is proportional to the rate of change of the corresponding period with $\psi$, and must therefore vanish whenever the period has a maximum or minimum. Secondly, the total couple must vanish for $H$ along each of the symmetry directions ([100], [110] and [111]). The vanishing comes about, however, in a more subtle way for the [110] and [111] directions than for [100]. Thus for $\psi = 45°$ in the (100) plane (i.e. $H$ along [110]), curve 1 has zero amplitude because the period has a maximum there, but the amplitudes of 2 and 3 become exactly equal and of opposite phase, so that the two terms just cancel each other. Evidently, then,

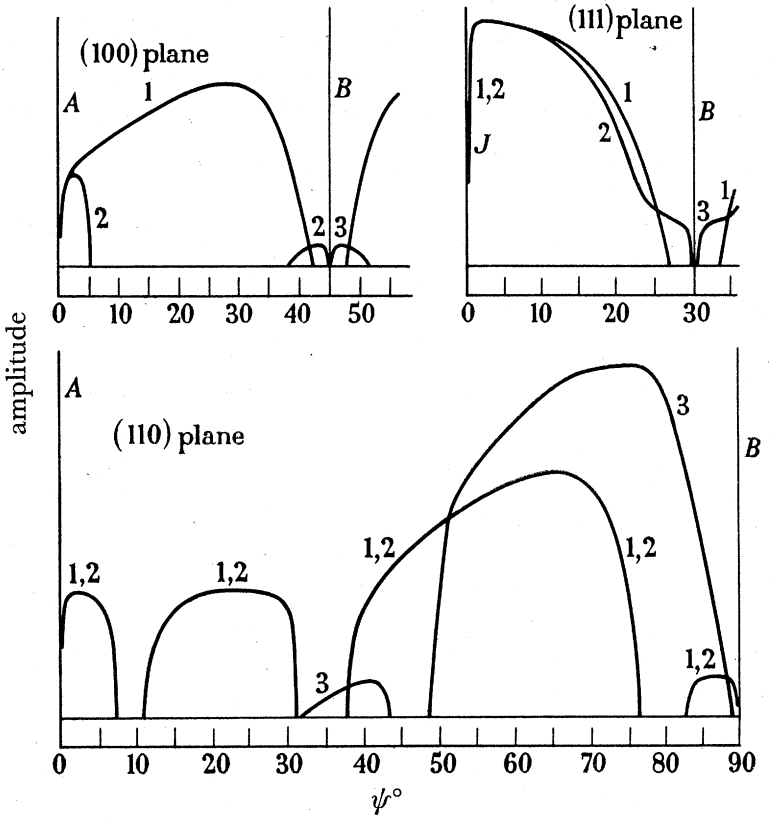


FIGURE 14. Schematic diagram showing the variation with $\psi$ of the amplitude of the high-frequency terms. The horizontal lines indicate the level of the smallest amplitude detectable.

the observed amplitude should become small over only a very narrow range of $\psi$. This range may indeed be so narrow as to be missed altogether; this appears to have happened at $\psi = 54{\cdot}4°$ in the (110) plane (i.e. $H$ along [111]), where theoretically the amplitudes of 1 and 2 should together be just equal to that of 3, but in antiphase. For curve 1, 2 in the (110) plane a possible explanation of some of the regions of small amplitude is that the plane of rotation of $H$ was not exactly (110) so that the two nominally coincident terms occasionally went out of phase by 180°. Finally, it should be noted that the theory suggests a strong general trend towards smaller amplitudes as the period becomes shorter.

### (*c*) *The dependence of oscillation amplitudes on temperature*

According to Lifshitz & Kosevich's calculations, the slope of a graph of $\ln(a/T)$ against $T$ (where $a$ is the amplitude) should be $-2\pi^2 k/(eh/2\pi mc)$, where $m$ is an effective mass given by

$$m = \frac{1}{2\pi}\left(\frac{\partial A}{\partial E}\right)_0,$$

$A$ means the maximum area of cross-section of the energy surface of energy $E$ (i.e. $\mathscr{A}$ is the value of $A$ for $E = E_0$), and the derivative is taken at the energy $E_0$ of the Fermi surface. In principle if $m$ were known for all orientations it should be possible to deduce the velocity of the electrons at the Fermi surface. In practice, however, $m$ can be determined at all accurately only for oscillations which do not contain more than one component, and a major investigation would be required to separate out the temperature-dependence of each component of the more complicated oscillations which are usually observed. Thus only

TABLE 5. MEASUREMENTS OF $(eh/2\pi mc)$ AND $E_0'$ IN A (100) PLANE

| | low-frequency oscillations | | | high-frequency oscillations | | |
|---|---|---|---|---|---|---|
| $\psi°$ | $10^{20}\frac{eh}{2\pi mc}$ | $10^7\Delta(1/H)$ | $10^{14}E_0'$ (erg) | $10^{20}\frac{eh}{2\pi mc}$ | $10^7\Delta(1/H)$ | $10^{14}E_0'$ (erg) |
| 0·0 | — | — | — | 12·5 | 2·58 | 48·5 (3·5) |
| 0·8 | 19·1 | 36·0 | 5·3 (0·2) | — | — | — |
| 1·4 | 19·5 | 36·0 | 5·4 (0·2) | 11·4 | 2·60 | 44·0 (3·0) |
| 16·2 | 19·3 | 36·3 | 5·3 (1·0) | 11·7 | 3·11 | 37·7 (2·9) |
| 25·0 | 19·3 | 36·0 | 5·3 (0·8) | 13·8 | 3·33 | 41·5 (2·7) |
| 30·2 | 17·0 | — | — | 13·2 | 3·41 | 38·6 (3·6) |
| 42·2 | 17·3 | — | — | 12·7 | 3·52 | 36·1 (4·9) |

*Note.* The figures in brackets are estimates of the possible errors in $E_0'$; these combine the errors in period and in $eh/2\pi mc$; the latter are of order 5 to 10 %. No estimates of $E_0'$ are given for the low frequency oscillations at $\psi = 30{\cdot}2°$ and $42{\cdot}2°$, since it is uncertain which one of the two periods is involved.

a very limited investigation was made for a few orientations in a (100) plane and the results are summarized in table 5; they are in general agreement with the more limited results of Shoenberg (1952). If $eh/2\pi mc$ is divided by the period, a quantity $E_0'$ is obtained which, for ellipsoidal energy surfaces, would be independent of orientation and equal to $E_0$, the Fermi energy measured relative to the highest (or lowest) energy of the band. In fact, $E_0$ varies with $\psi$ (though not very significantly for the low-frequency oscillations); this is not very surprising since we know that the energy surfaces are not ellipsoidal. Probably, however, $E_0'$ does correctly represent the order of magnitude of $E_0$, the Fermi energy.

### (*d*) *The effect of alloying with magnesium*

To investigate whether the oscillations in aluminium are caused by electrons or positive holes, some measurements were carried out on the dependence of period on the quantity of magnesium dissolved in solid solution in the aluminium crystals. These period measurements were made at orientations where only one low-frequency or high-frequency term was present, so that a good accuracy ($\sim 1$ %) could be achieved. Table 6 shows that there is no significant dependence of high-frequency period on the concentration of magnesium (up to 0·26 % by weight) in aluminium, but that the low-frequency period at about $\psi = 1°$ in a (100) plane increases with the quantity of magnesium; higher concentrations could not

be used owing to the rapid decrease of amplitude with increasing concentration. The rise in low-frequency period corresponding to a nominal concentration of 0·26 % by weight of magnesium is about 2·3 %. An attempt was made to check the concentration of magnesium in two of the specimens (crystals *A* and *B*), but owing to their small masses, only a low accuracy could be achieved; the analysis indicated that both nominal 0·26 % specimens contained (0·2 ± 0·1) % of magnesium. However, the fact that the oscillation amplitude in crystal *B* was only about half that in crystal *A* suggested that if *B* contained the same quantity of magnesium as *A*, then either some of the magnesium in *A* was not in solid solution, or else *B* was badly distorted.

Since adding magnesium to aluminium effectively decreases the number of electrons per atom, this observed rise in low-frequency period (i.e. decrease in maximum cross-sectional

TABLE 6. VARIATION OF PERIOD AND AMPLITUDE WITH ADDITION OF MAGNESIUM

$10^7\Delta(1/H)$ ($G^{-1}$)

| specimen | $\psi$° | low frequency | high frequency | relative low-frequency amplitude |
|---|---|---|---|---|
| pure | 0·8 | 36·10 } *35·98 ± 0·13* | 2·59 | 100 |
| | 1·4 | 35·85 } | | |
| | 25 | — | 3·33 | |
| | 70 | — | 3·21 | |
| 0·08 % Mg | 0·8 | 36·25 } *36·35 ± 0·10* | 2·61 | 20 |
| | 1·4 | 36·45 } | 2·62 | |
| | 25 | — | 3·32 | |
| 0·26 % Mg (*A*) | 0·8 | 36·82 | 2·52 | 7 |
| | 1·4 | 36·69 | — | |
| | 25 | — *36·81 ± 0·13* | 3·34 | |
| | 70 | — | 3·20 | |
| 0·26 % Mg (*B*) | 0·8 | 36·72 | 2·58 | 4 |
| | 1·4 | 37·09 | — | |
| | 25 | — | 3·34 | |
| | 70 | — | 3·20 | |

*Note.* Average values of the low-frequency periods for the various concentrations together with estimates of the errors are indicated by italics above; the errors are standard deviations calculated from the various individual determinations made in each group (five in each except for the 0·08 % alloy for which there were only two). The estimated errors of the high-frequency periods were of order 0·05.

area of the Fermi surface pocket) can be interpreted as meaning that the low-frequency de Haas–van Alphen oscillations are caused by electrons rather than by positive holes. A detailed discussion of the interpretation of this and previous experiments on the effect of alloying has been given by Heine (1956).

I should like to express my gratitude to Dr D. Shoenberg, F.R.S., for the guidance, encouragement and advice he has freely given throughout the experimental work and during the preparation of this paper. I should like to thank Mr V. Heine for informing me of some of his theoretical ideas before publication, and in particular for introducing me to the symmetry arguments on p. 310 which opened the way to a detailed analysis of the results. My thanks are also due to Dr R. G. Chambers for many helpful discussions during the experiments, to Dr A. B. Pippard, F.R.S., and Dr J. W. Glen for some helpful discussions related to the interpretation of the results, and to Dr J. Ashmead, Mr F. Sadler and the

technical staff of the laboratory for making available excellent liquid helium facilities during approximately one hundred helium runs. Finally, I should like to express my gratitude to the Rutherford Memorial Committee of the Royal Society for the generous financial support provided during the three years from October 1952 to October 1955 by the first Rutherford Memorial Postgraduate Scholarship.

## References

Croft, G. T., Donahoe, F. J. & Love, W. F. 1955 *Rev. Sci. Instrum.* **26**, 360.
Dingle, R. B. 1952 *Proc. Roy. Soc.* A, **211**, 517.
Heine, V. 1956 *Proc. Phys. Soc.* A, **69**, 505.
Heine, V. 1957 (Submitted to *Proc. Roy. Soc.*)
Landau, L. D. 1939 See appendix to Shoenberg (1939).
Lifshitz, I. M. & Kosevich, A. M. 1954 *Dokl. Akad. Nauk. SSSR*, **96**, 963.
Lifshitz, I. M. & Kosevich, A. M. 1955 *J. Exp. Theor. Phys. USSR*, **29**, 730.
Lifshitz, I. M. & Pogorelov, A. V. 1954 *Dokl. Akad. Nauk. SSSR*, **96**, 1143.
Mott, N. F. & Jones, H. 1936 *Theory of the properties of metals and alloys*, p. 157. Oxford University Press.
Onsager, L. 1952 *Phil. Mag.* **43**, 1006.
Pippard, A. B. 1955 *Proceedings of the 10th Solvay Congress* (1954), *Brussels*.
Shoenberg, D. 1939 *Proc. Roy. Soc.* A, **170**, 341.
Shoenberg, D. 1952 *Phil. Trans.* A, **245**, 1.


PHILOSOPHICAL TRANSACTIONS OF THE ROYAL SOCIETY A MATHEMATICAL, PHYSICAL & ENGINEERING SCIENCES